RAA 2018 Vol. **18** No. **11**, 133(12pp) doi: 10.1088/1674–4527/18/11/133
© 2018 National Astronomical Observatories, CAS and IOP Publishing Ltd.
http://www.raa-journal.org *http://iopscience.iop.org/raa*

Research in Astronomy and Astrophysics

Analysis of the wide area differential correction for BeiDou global satellite navigation system

Ran Li[1,2], Yue-Ling Cao[1,3], Xiao-Gong Hu[1,3], Cheng-Pan Tang[1,3], Shan-Shi Zhou[1,3], Xin Meng[4], Li Liu[5], Ran-Ran Su[5] and Zhi-Qiao Chang[5]

[1] Shanghai Astronomical Observatory, Chinese Academy of Sciences, Shanghai 200030, China; *caoyueling@shao.ac.cn*
[2] University of Chinese Academy of Sciences, Beijing 100049, China
[3] Shanghai Key Laboratory of Space Navigation and Position Techniques, Shanghai 200030, China
[4] College of Surveying and Geo-Informatics, Tongji University, Shanghai 200092, China
[5] Beijing Global Information Application and Development Center, Beijing 100094, China

Received 2018 March 9; accepted 2018 May 19

Abstract The regional BeiDou Satellite System, or BDS2, broadcasts a differential correction as Equivalent Satellite Clock Correction to correct both orbit and satellite clock errors. For the global BDS, or BDS3, satellite orbit and clock corrections conforming with RTCA standards will be broadcast to authorized users. The hybrid constellation and regional monitoring network pose challenges for the high precision separation of orbit and satellite clock corrections. Three correction models of kinematic, dynamic and Two-way Satellite Time Frequency Transfer (TWSTFT)-based dynamic were studied to estimate the satellite orbit and clock corrections. The correction accuracy of the three models is compared and analyzed based on the BDS observation data. Results show that the accuracies (root mean square, RMS) of dual-frequency real-time positioning for the three models are about 1.76 m, 1.78 m and 2.08 m respectively, which are comparable with the performance of WAAS and EGNOS. With dynamic corrections, the precision of Precise Point Positioning (PPP) experiments may reach about 23 cm after convergence.

Key words: celestial mechanics — methods: data analysis — space vehicles

1 INTRODUCTION

To improve the positioning accuracy of a satellite navigation system, many countries or regions have established a Satellite-Based Augmentation System (SBAS) for GPS and GLONASS, including the American Wide Area Augmentation System (WAAS), European Geostationary Navigation Overlay System (EGNOS), Japanese MTSAT Satellite-Based Augmentation System (MSAS), Indian GPS Aided GEO Augmented Navigation (GAGAN) and so on (Lawrence et al. 2007; Manabe 2008; Seynat et al. 2009). These SBASs are equipped with signal transponders via geosynchronous equatorial orbit (GEO) satellites, providing real-time orbit correction, clock correction and grid ionospheric correction to authorized users. Next-generation standard, dual-frequency, multi-constellation (DFMC) SBASs have been proposed in the SBAS Interoperability Working Group, to employ dual-frequency signals of multi-constellation GNSSs. DFMC SBAS users can eliminate most ionospheric delay by relying on dual-frequency signals, in which no information on ionospheric delay is broadcast and more satellites from multi-constellation GNSS may be used for augmentation purposes. The BeiDou Satellite System (BDS2) participates in the design of next-generation DFMC SBAS standards. Unlike other SBASs, for regional BDS SBAS, orbit and clock corrections are combined into one, as the equivalent satellite clock correction, to make the processing simple. The disadvantage

of the method, ignoring the satellite orbit error in different projection directions, leads to a reduction in correction accuracy when the satellite orbit error is large. To improve the correction accuracy, the next-generation of BDS SBAS will provide both satellite orbit and satellite clock corrections. Since we focus on the study of orbit and satellite clock correction for DFMC SBAS, grid ionospheric correction will not be discussed in this paper.

For the algorithms that perform orbit and clock correction in SBAS, experts and scholars have conducted some research studies, in which WAAS uses the snapshot algorithm and kinematic observation equation combined with a Kalman filter to calculate the satellite orbit and clock correction (Tsai 1999). Thales Alenia Space has developed new orbit determination and synchronization modules for EGNOS; the newly proposed orbit determination module is based on real time processing using only code carrier measurement; the new synchronization module solves clock errors directly referencing GPS time scale; for the stations and satellites, it uses both code carrier and phase carrier measurements as well as orbits estimated by the orbit determination process (Labé et al. 2016). Cao applied independent two-way time synchronization observation to realize the precision separation of orbit and clock correction (Cao et al. 2014). To meet the requirement of sub-meter level positioning service for BDS SBAS, a new concept of zone correction was proposed by Chen; after applying zone correction, the Precise Point Positioning (PPP) precision was below 0.15 m horizontally and 0.20 m vertically for a dual-frequency user at a distance of 600 km off the zone center (Chen et al. 2017).

2 DYNAMIC WIDE AREA DIFFERENTIAL CORRECTION MODEL

Satellite orbit error exhibits slow and systematic change. Therefore, it is possible to precisely determine the satellite orbit and then fix the satellite orbit as a known value to determine the satellite clock offset through the pseudorange and carrier-phase observations. In this manner, the residual error of the satellite orbit will be combined into the satellite clock offset, thereby guaranteeing consistency of the differential correction. This method divides the differential correction into two independent parts, namely, the dynamic orbit correction and the dynamic clock correction, which may also reduce the required computer memory and improve the operation speed.

The calculation processing of the dynamic wide area differential correction model (DYN) is shown in Figure 1.

2.1 Dynamic Orbit Correction

BDS uses the Two-way Satellite Time Frequency Transfer (TWSTFT) measurement to directly measure the satellite clock offset relative to BeiDou Time (BDT) (Cao et al. 2014). The TWSTFT satellite clock fixed orbit determination strategy is applied to generate a precisely determined satellite orbit as well as a predicted satellite orbit. Details about the orbit determination are described in Tang et al. (2016); Zhou et al. (2011), and they show that this orbit determination strategy can improve the User Equivalent Range Error (UERE) of GEO and Inclined Geosynchronous Satellite Orbit (IGSO) satellites. It is necessary to extrapolate the satellite orbit since the BDS SBAS provides real-time service. As the satellite orbit error changes slowly, we process the orbit determination strategy hourly. An orbit prediction of one hour is used to compare with the broadcast ephemeris orbit, and the orbit correction is calculated with Equation (1)

$$(\Delta x, \Delta y, \Delta z) = \mathrm{orbit}_{\mathrm{TWSTFT-based}} - \mathrm{orbit}_{\mathrm{eph}} \ , \quad (1)$$

where $(\Delta x, \Delta y, \Delta z)$ is the three-dimensional (3D) orbit correction, $\mathrm{orbit}_{\mathrm{TWSTFT-based}}$ is the predicted orbit from the TWSTFT satellite clock fixed orbit determination strategy and $\mathrm{orbit}_{\mathrm{eph}}$ is the orbit computed through broadcast ephemeris.

2.2 Dynamic Clock Correction

$$\begin{aligned} PC =& |X^{\mathrm{sat}} - X_{\mathrm{rcv}}| + c(\delta t_r - \delta t_s) \\ &+ \rho_{\mathrm{trop}} + \rho_{\mathrm{com}} + \varepsilon_\rho \ , \\ LC =& |X^{\mathrm{sat}} - X_{\mathrm{rcv}}| + c(\delta t_r - \delta t_s) + \rho_{\mathrm{trop}} \\ &+ \rho_{\mathrm{com}} + \lambda N + \varepsilon_L \ . \end{aligned} \quad (2)$$

Dual frequency ionosphere-free pseudorange and carrier phase combinations are used to generate a precise satellite clock in the processing of dynamic clock correction. The measurement equation is given as Equation (2), where PC and LC are ionospheric-free pseudorange and carrier phase combinations, respectively. X^{sat} is the satellite position vector, X_{rcv} is the precisely known monitor receiver coordinates, and δt_s and δt_r are the satellite and receiver clock, respectively. ρ_{trop} is the tropospheric delay, ρ_{com} indicates the common error, including the satellite transmitting phase center correction,

receiver eccentricity correction, tidal correction and periodic relativistic clock correction, which could be corrected following proper models. ε is the multipath and observation noise. λN is carrier phase ambiguity.

Given X^{sat} as the fixed value to generate the predicted orbit, the processing estimates epoch-by-epoch satellite and receiver clocks using a data arc of 24 hours. Measurement errors such as tropospheric delay that cannot be precisely modeled are treated as unknown parameters, while the phase ambiguities are estimated as real numbers rather than integers.

Considering the fast-changing characteristics of satellite clock offset, the strategy of precise satellite clock processing will be operated every ten minutes. Post-processing satellite clock corrections are obtained from the difference between the last ten-minute precise satellite clock offset and the broadcast satellite clock, and it will be predicted with a linear model for real-time users.

3 KINEMATIC WIDE AREA DIFFERENTIAL CORRECTION MODEL

BDS2 broadcasts one-dimensional differential correction, as equivalent satellite clock correction to authorized users (BeiDou ICD 2013). Separating the satellite clock and orbit corrections, four-dimensional differential correction processing with the kinematic method is proposed in this paper.

Station clock, satellite clock offset and orbit radial errors are highly correlated in kinematic observation Equation (3); the normal equations would be seriously ill-conditioned if they were solved simultaneously. The solution would have large deflection compared with the true value. The processing of kinematic wide area differential correction (KIN) computation is illustrated in Figure 2, which is different from the dynamic strategy because it calculates the satellite clock correction first.

3.1 Kinematic Clock Correction

Dual frequency ionosphere-free pseudorange residual is computed by removing geometric range, satellite clock offset and tropospheric delay from the Code Noise and Multipath Correction (CNMC) smoothed pseudorange (Wu et al. 2012; Cao et al. 2012) and can be simplified as

$$\Delta\rho_i^j = c\delta t_i - \varepsilon_{\mathrm{orb}} - \varepsilon_{\mathrm{satclk}} + \varepsilon_i^j \ , \tag{3}$$

where $\Delta\rho_i^j$ is the pseudorange residual, $c\delta t_i$ is the station clock offset, and $\varepsilon_{\mathrm{orb}}$ and $\varepsilon_{\mathrm{satclk}}$ are orbit and satellite clock offsets in broadcast ephemeris, respectively.

According to Cao et al. (2012), the equivalent satellite clock correction 'ESclkcor' is used to correct satellite clock errors and orbit radial errors as well as average projection of orbit tangential and normal errors in combination, given by Equation (4)

$$\mathrm{ESclkcor} = \varepsilon_{\mathrm{orb}} + \varepsilon_{\mathrm{satclk}} \ . \tag{4}$$

The station clock and equivalent satellite clock correction will be unknown parameters and solved with least-squares estimation.

3.2 Kinematic Orbit Correction

As equivalent satellite clock correction does not take into account the effect of orbit error projection difference, the residual orbit error is estimated with the pseudorange residual correction, and the equivalent satellite clock correction and station clock are solved.

$$\begin{aligned} \delta\varepsilon_{\mathrm{orb}} &= \Delta\rho_i^j - c\delta t_i + \mathrm{ESatcor} \\ &= a_i \cdot x + b_i \cdot y + c_i \cdot z \ , \end{aligned} \tag{5}$$

where $\delta\varepsilon_{\mathrm{orb}}$ is the orbit projection error, and a_i, b_i and c_i are the orbit error projection coefficients.

If no cycle slip is detected, the epoch-differenced carrier phase residual is also used to compute the epoch-wise variation of the satellite orbit errors.

$$\Delta L_i^j = c\delta t_i - \delta\varepsilon_{\mathrm{orb}i} - \mathrm{ESatcor}_i + \lambda N + \varepsilon_i^j \ , \tag{6}$$

$$\begin{aligned} d\Delta L_i^j =& c(d\delta t_i) - (\delta\varepsilon_{\mathrm{orb}i} - \delta\varepsilon_{\mathrm{orb}i-1}) \\ & - (\mathrm{ESatcor}_i - \mathrm{ESatcor}_{i-1}) + \Delta\varepsilon_i^j \ , \end{aligned} \tag{7}$$

where ΔL_i^j is the dual-frequency ionosphere-free carrier phase residual and $d\Delta L_i^j$ is the epoch-differenced carrier phase residual. $d\delta t$ is the epoch-differenced station clock, which can be achieved using multiple common satellites (Cao et al. 2012; Chao 1997).

Ignoring the variation of epoch orbit error projection coefficients, the epoch-wise variation of the satellite orbit errors could be estimated with Equation (8)

$$\begin{aligned} d\tilde{\Delta} L_i^j &= d\Delta L_i^j - c(d\delta t_i) + \mathrm{dESatcor} \\ &= a_i(x_i - x_{i-1}) + b_i(y_i - y_{i-1}) + c_i(z_i - z_{i-1}) \\ &= a_i dx_{\phi,i} + b_i dy_{\phi,i} + c_i dz_{\phi,i} \ . \end{aligned} \tag{8}$$

The Minimum Variance (MV) estimation approach is adopted for orbit error estimation, which is less sensitive to the observing geometry and measurement noise (Tsai 1999).

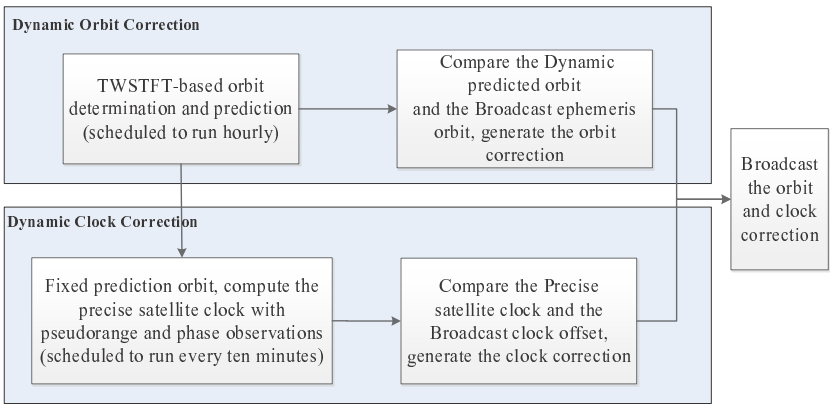

Fig. 1 Processing of the DYN model.

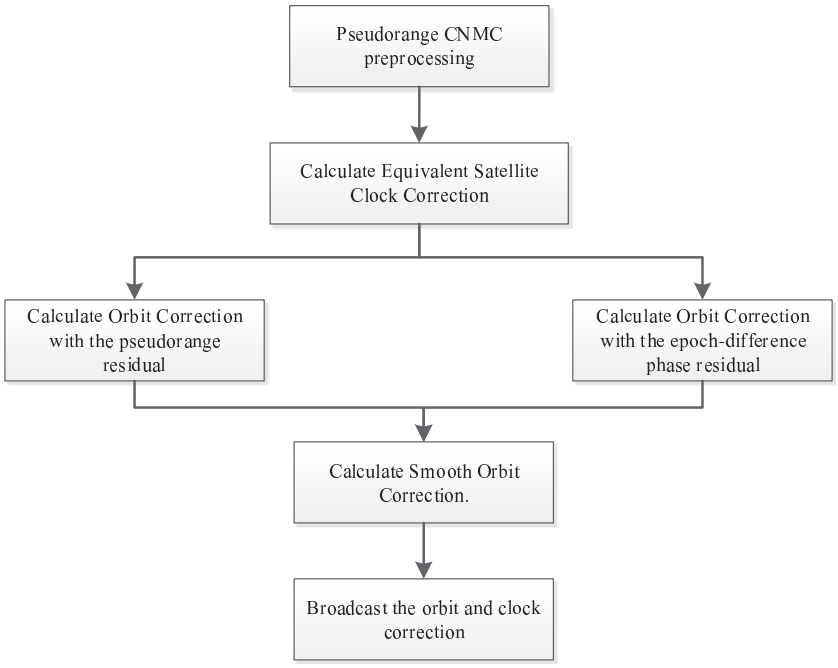

Fig. 2 Processing of the KIN model.

The pseudorange-based satellite orbit $x_{c,i}$ is taken as the virtual observation of the actual parameters as follows

$$v_{c,i} = x_i - x_{c,i} \ , \tag{9}$$

where x_i is the true value of the satellite orbit at epoch i and $v_{c,i}$ is the residual.

The phase-based epoch-wise variation of satellite orbit $dx_{\phi,i}$ is also regarded as the virtual observation of the actual parameters.

$$v_{\Delta\phi,i} = (x_i - x_{i-1}) - dx_{\phi,i} \ , \tag{10}$$

where $(x_i - x_{i-1})$ is the true value of the epoch-wise variation of the satellite orbit at epoch i and $v_{\Delta\phi,i}$ is the residual.

By combining Equation (9) and Equation (10), we can obtain the smoothed orbit error correction (Chen et al. 2017).

4 DYNAMIC WIDE AREA DIFFERENTIAL CORRECTION MODEL BASED ON TWSTFT

For the TWSTFT-based dynamic wide area differential correction model (TSDYN), the processing of the satellite orbit correction is the same as in Section 2.1. The satellite clock correction is calculated based on comparisons between the real-time TWSTFT clock offset and the broadcast satellite clock offset.

For detailed processing of the real-time TWSTFT clock offset, refer to Liu et al. (2009), which indicates

that the precision of the satellite clock estimation from TWSTFT measurements is better than 1 ns.

5 EXPERIMENTS AND DISCUSSION

The correction accuracies of the three wide area differential correction models are compared with BDS observation data from China's regional monitoring network, in the form of User Differential Range Error (UDRE), real-time positioning accuracy and precise positioning accuracy. The performance of BDS SBAS is also compared with other SBASs such as WAAS and EGNOS.

5.1 Comparison of Three Wide Area Differential Correction Models

Based on the analysis of three wide area differential correction algorithms, Table 1 summarizes the differences among the three differential correction models.

As seen from Table 1, the kinematic correction model uses pseudorange and epoch-difference carrier phase observation to calculate the satellite orbit and clock correction epoch by epoch. The dynamic model calculates the satellite orbit and clock correction in batch processing with 24-hour data.

5.2 User Differential Range Error (UDRE)

UERE under open service and UDRE corrected by the three models of differential corrections were calculated and compared with BDS observation data on 2016 July 27. To compare the performance among the different wide area difference models, all three wide area differential models are used with BeiDou observation data from China's regional monitoring network, and the stations are distributed in Beijing, Sanya, Chengdu, Kashi, Harbin and Urumqi.

The formulas for the UERE and UDRE calculation are as follows

$$\begin{aligned} \mathrm{UERE} =& PC - \left|X^{\mathrm{sat}} - X_{\mathrm{rcv}}\right| - c(\delta t_r - \delta t_s) \\ & - \rho_{\mathrm{trop}} - \rho_{\mathrm{cor}} \ , \\ \mathrm{UDRE} =& PC - \left|X^{\mathrm{sat}} - X_{\mathrm{rcv}}\right| - c(\delta t_r - \delta t_s) \\ & - \rho_{\mathrm{trop}} - \rho_{\mathrm{cor}} - \Delta\mathrm{pcor} \ . \end{aligned} \tag{11}$$

ρ_{cor} is the systematic errors in length, which can be modeled precisely. According to the system design, Δpcor is the differential correction and is provided to authorized users only to correct their pseudorange observations; for the meanings of other variables, please refer to Equation (2).

Figure 3 displays the statistics associated with UERE and UDRE for all the visible satellites from six monitoring stations in China, where $\mathrm{UERE}_{\mathrm{os}}$ is the open service UERE, $\mathrm{UDRE}_{\mathrm{kin}}$ is the UERE with kinematic differential correction, $\mathrm{UDRE}_{\mathrm{dyn}}$ is the UERE with dynamic differential correction and $\mathrm{UDRE}_{\mathrm{dynTS}}$ is the UERE with TWSTFT-based dynamic differential correction.

This demonstrate that the three models of differential corrections all effectively improve the user range accuracy compared with UERE under open service.

Table 2 gives the details of statistics for UERE and UDRE resulting from the six monitoring stations.

The statistical results indicate that the average UDRE is improved by 35%, 40% and 34% for the kinematic correction model, dynamic correction model and TWSTFT-based dynamic correction model respectively, compared with the average UERE under open service.

5.3 Dual-frequency Real-time Positioning Accuracy with BDS SBAS Corrections

Dual frequency ionosphere-free pseudorange is used to compute the real-time positioning. The observation equations under open service and SBAS service are respectively defined as follows

$$\begin{aligned} PC_{\mathrm{open}} =& |X^{\mathrm{sat}} - X_{\mathrm{rcv}}| + c(\delta t_r - \delta t_s) \\ & + \rho_{\mathrm{trop}} + \rho_{\mathrm{com}} + \varepsilon_{\rho} \ , \end{aligned} \tag{12}$$

$$\begin{aligned} PC_{\mathrm{SBAS}} =& |X^{\mathrm{sat}} - X_{\mathrm{rcv}}| + c(\delta t_r - \delta t_s) + \rho_{\mathrm{trop}} \\ & + \rho_{\mathrm{com}} + \varepsilon_{\rho} - \varepsilon_{\mathrm{orb}} - \varepsilon_{\mathrm{satclk}} \ , \end{aligned} \tag{13}$$

where PC_{open} is the ionospheric-free pseudorange measurement under open service; PC_{SBAS} is the ionospheric-free pseudorange measurement under SBAS service; $\varepsilon_{\mathrm{orb}}$ and $\varepsilon_{\mathrm{satclk}}$ are orbit and satellite clock differential correction; for the meanings of other variables, please refer to Equation (2).

With precisely known coordinate monitoring station data, the real-time position coordinates are estimated and compared with the precise coordinates. The position errors are analyzed under open service and SBAS service with three models of differential corrections. The dual-frequency real-time positioning results for 24 hours are shown in Figure 4.

Table 3 indicates that the positioning accuracy is improved by 31%, 32% and 24% for the kinematic correction model, dynamic correction model and TWSTFT-based dynamic correction model respectively, corresponding to open service.

Table 1 The Differences of Three Wide Area Differential Correction Models

	Kinematic	Dynamic	TWSTFT-based
Clock correction	Based on the pseudorange observation, epoch-by-epoch processing	Based on pseudorange and carrier phase observation, batch processing with 24 hour data	Based on real-time TWSTFT clock offset, epoch-by-epoch processing
Orbit correction	Based on the pseudorange and epoch-difference carrier phase observation, epoch-by-epoch processing	Based on pseudorange and carrier phase observation, batch processing with 24 hour data	Based on pseudorange and carrier phase observation, batch processing with 24 hour data
Observation data	Phase-smoothed pseudorange and epoch-difference carrier phase observations	Raw pseudorange and carrier phase observations	Real-time TWSTFT clock offset, raw pseudorange and carrier phase observations
Ambiguity processing method	Eliminated with epoch differenced method	Estimate	Estimate
Tropospheric parameter	The Saastamoinen model	Estimated every three hours	Estimated every three hours

Table 2 The RMS of UDREs

	UEREos (m)	$\mathrm{UDRE}_{\mathbf{kin}}$ (m)	$\mathrm{UDRE}_{\mathbf{dyn}}$ (m)	$\mathrm{UDRE}_{\mathbf{dynTS}}$ (m)
Beijing	0.91	0.53	0.48	0.52
Sanya	1.07	0.78	0.59	0.70
Kashi	0.91	0.66	0.66	0.73
Chengdu	0.87	0.57	0.54	0.63
Harbin	0.85	0.50	0.50	0.53
Urumqi	0.90	0.58	0.54	0.58
Average	0.92	0.60	0.55	0.62

In order to verify the reliability of the three differential correction models, we select 12 stations in China to estimate the real-time positioning accuracy. The distribution of the stations is shown in Figure 5.

The daily average positioning accuracy of 12 stations is listed in Table 4 from 2017 May 6 to 2017 May 11.

It indicates that the real-time positioning accuracy of the three differential correction models is reliable. After applying differential correction, the average 3D real-time positioning root mean square (RMS) values of all three models are below 2 meters.

5.4 The Performance of WAAS and EGNOS

To compare BDS SBAS orbit and satellite clock correction accuracy with other SBASs, the performances of WAAS and EGNOS are established, just considering the orbit and clock corrections. The EGNOS differential corrections can be downloaded via FTP at *ftp://ems.estec.eas.int/* and the WAAS differential corrections can be downloaded via FTP at *ftp://nstb.tc.faa.gov/*. GPS users with WAAS/EGNOS capable receivers will be able to perform differential positioning across the United States and Europe.

The observation data from IGS stations within the coverage of EGNOS and WAAS were selected on 2016 July 27. With WAAS orbit and clock differential corrections, dual-frequency real-time positioning accuracies of stations amc2, whc1, widc, gode, gol2 and holp distributed in the United States were estimated. With EGNOS orbit and clock differential corrections, the dual-frequency real-time positioning accuracies of stations hueg, sofi, gras, bzrg, glsv and hert distributed in Europe were estimated.

Figure 6 gives the comparison of real-time positioning accuracy of GPS and WAAS, and Figure 7 shows the real-time positioning accuracy of GPS and EGNOS.

Table 5 presents the statistics of the positioning errors from Figures 6 and 7. In addition, BDS real-time positioning accuracy resulting from Section 5.3 is also listed to compare with WAAS and EGNOS.

The results indicate that the real-time positioning accuracy of BDS SBAS is comparable with WAAS and EGNOS, and WAAS has slightly higher precision.

5.5 Real-Time PPP Using BDS SBAS Corrections

Rho and Langley investigated the use of WAAS corrections for PPP. They successfully applied WAAS orbit and

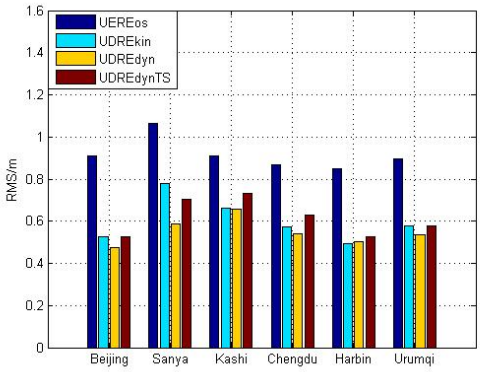

Fig. 3 UDREs of the six monitoring stations.

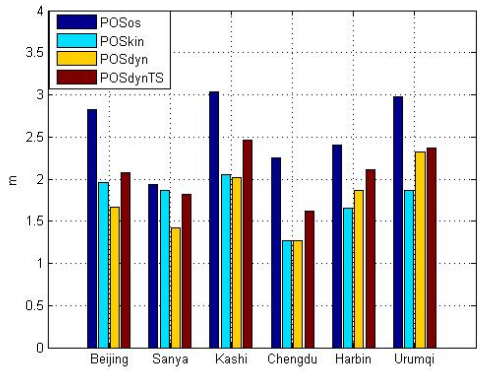

Fig. 4 Dual-frequency real-time positioning RMS (a *blue bar* indicates the no-differential model; an *aqua bar* signifies the kinematic correction model; a *yellow bar* represents the dynamic correction model; and a *red bar* stands for the TWSTFT-based dynamic correction model).

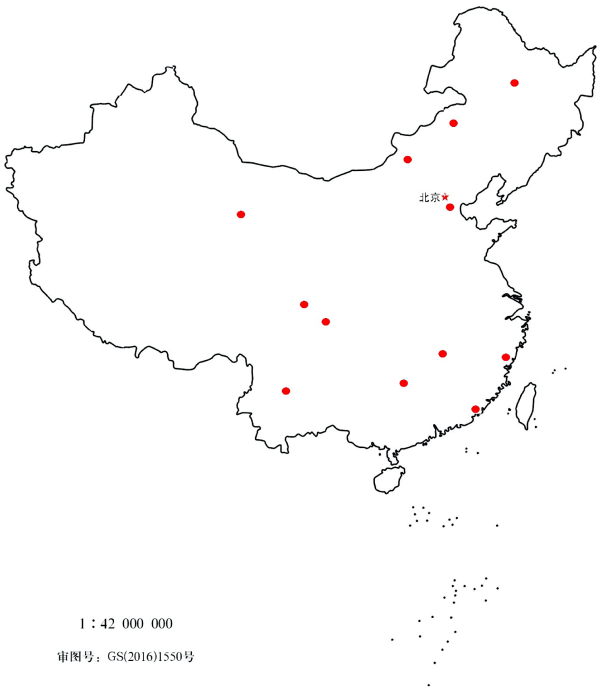

Fig. 5 Distribution of the 12 stations.

Table 3 The Statistics of Dual-frequency Real-time Positioning Accuracy

Station	Open service (m)		Kinematic model (m)		Dynamic model (m)		TWSTFT-based dynamic model (m)	
	Vertical RMS	3D RMS	Vertical RMS	3D RMS	Vertical RMS	3D RMS	Vertical RMS	3D RMS
Beijing	2.28	2.82	1.75	1.96	1.48	1.67	1.84	2.08
Sanya	1.55	1.94	1.73	1.87	1.09	1.42	1.41	1.82
Kashi	2.32	3.04	1.72	2.05	1.72	2.02	2.08	2.46
Chengdu	1.62	2.25	0.97	1.27	1	1.27	1.3	1.62
Harbin	1.55	2.4	1.39	1.65	1.33	1.87	1.53	2.11
Urumqi	2.66	2.98	1.65	1.86	2.13	2.32	2.11	2.37
Average	2	2.57	1.54	1.78	1.46	1.76	1.71	2.08

Table 4 Dual-frequency Real-time Positioning Accuracy of 12 Stations

Data	Open service (m)	Kinematic model (m)	Dynamic model (m)	TWSTFT-based dynamic model (m)
5.6	2.48	1.72	1.87	1.98
5.7	2.37	1.71	1.91	2.04
5.8	2.66	1.91	1.87	1.87
5.9	2.51	1.78	1.88	2.05
5.10	2.48	1.71	1.88	1.88
5.11	2.26	1.69	1.94	1.99
Average	2.46	1.75	1.89	1.97

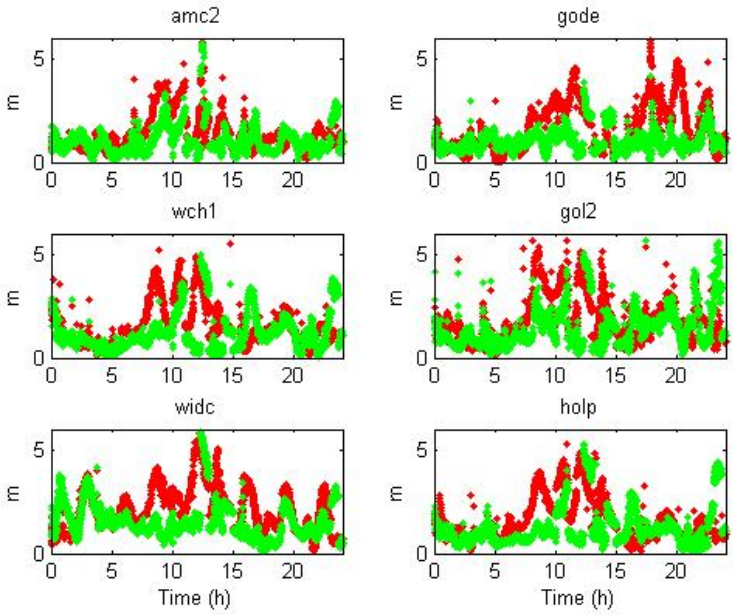

Fig. 6 Dual-frequency real-time positioning: use of the GPS broadcast ephemeris (in *red*) and use of the GPS broadcast ephemeris and WAAS differential corrections (in *green*).

clock corrections to correct carrier phase observation in PPP processing and obtained centimeter-level accuracy in horizontal positioning from statistics associated with a 24-hour interval (Rho & Langley 2007; Heßelbarth & Wanninger 2013).

To promote the development of the BDS real-time precise applications, the National BDS Augmentation Service System (NBASS) was established in 2014. With the real-time corrections estimated with 150 nationwide reference stations in China, BDS dual-frequency PPP

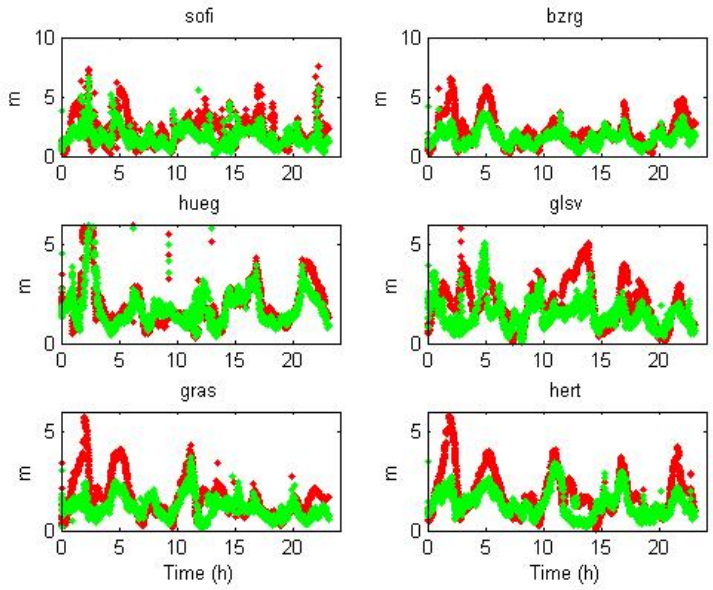

Fig. 7 Dual-frequency real-time positioning: use of the GPS broadcast ephemeris (in *red*) and use of the GPS broadcast ephemeris and EGNOS differential corrections (in *green*).

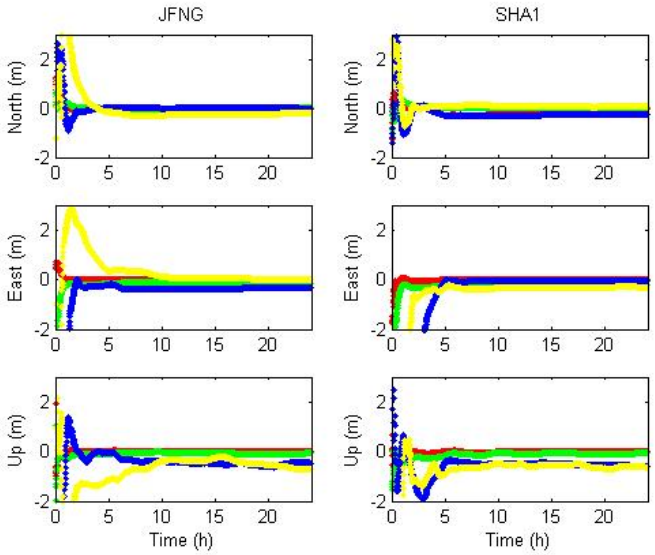

Fig. 8 PPP results with IGS products (*red*), kinematic wide area differential corrections (*blue*), dynamic wide area differential corrections (*green*) and TWSTFT-based dynamic wide area differential corrections (*yellow*) at station JFNG (*left*) and SHA1 (*left*) on 2016 July 27.

can achieve horizontal and vertical accuracies as high as 0.2 m and 0.3 m respectively, at the 95% confidence level (Shi et al. 2017).

In our study, we applied BDS SBAS orbit and clock corrections estimated with only six monitoring stations for PPP processing, and the stations are distributed in Beijing, Sanya, Chengdu, Kashi, Harbin and Urumqi. The PPP results with IGS post-precise satellite ephemeris and clock products were also analyzed as a reference.

The observation functions can be simplified as

$$\begin{aligned} PC =& |X^{\mathrm{sat}} - X_{\mathrm{rcv}}| + c(\delta t_r - \delta t_s) \\ &+ m \cdot ZTD + \varepsilon_\rho \ , \\ LC =& |X^{\mathrm{sat}} - X_{\mathrm{rcv}}| + c(\delta t_r - \delta t_s) \\ &+ m \cdot ZTD + \lambda N + \varepsilon_L \ , \end{aligned} \tag{14}$$

Table 5 The RMS of Dual-frequency Real-time Positioning with Differential Correction (unit: m)

WAAS station	widc	whc1	amc2	gode	gol2	holp	AVERAGE
GPS	2.38	1.9	1.63	2.04	2.13	1.88	1.99
GPS + WAAS	1.82	1.52	1.27	1.15	1.73	1.51	1.50
EGNOS station	hueg	sofi	gras	bzrg	glsv	hert	AVERAGE
GPS	2.43	2.48	1.93	2.44	2.26	2.17	2.29
GPS + EGNOS	2.16	1.81	1.3	1.68	1.64	1.52	1.69
BDS station	Beijing	Sanya	Kashi	Chengdu	Harbin	Urumqi	AVERAGE
BDS	2.82	1.94	3.04	2.25	2.4	2.98	2.57
BDS + BDS SBAS	1.67	1.42	2.02	1.27	1.87	2.32	1.76

where m and ZTD are mapping function and zenith tropospheric delay respectively; for the meanings of other variables, please refer to Equation (2). Errors resulting from the offset and variation of the antenna phase center, tidal displacements, relativity and phase wind-up at the satellite antenna are assumed to have been corrected by models. Table 6 summarizes the strategy for the PPP in the paper.

Satellite orbit and clock offset, which are used to compute geometrical distance in Equation (13), are achieved from BDS broadcast ephemeris and BDS SBAS differential corrections, or IGS post-precise satellite ephemeris and clock products respectively.

PPP performance with three models of differential corrections as well as IGS post-precise products was assessed with BDS data from stations as JFNG, GUA1, SHA1 and KUN1 on 2016 July 27. We also used BeiDou observation data from China's regional monitoring network, and the stations are distributed in Chengdu, Harbin, Urumqi and Shantou. All these stations are located in China and their coordinates are precisely known.

The time series of the PPP processing errors are shown in Figure 8, where blue lines signify results related to the kinematic correction model, green lines represent results from the dynamic correction model and yellow lines stand for results with the TWSTFT-based dynamic correction model. Red lines trace results with IGS post-precise products, which may be shown as a reference. The top subfigures give the positioning errors in the North-South direction, the middle subfigures show the positioning errors in the East-West direction and the bottom subfigures give the positioning errors in the Height direction.

According to the IGS post-precise products, the dynamic differential correction model shows the best convergence characteristic. The convergence time of the dynamic differential correction model needs about 80 min to achieve an accuracy better than 0.3 m. However, the convergence of the kinematic differential correction model needs more than 120 min to obtain an accuracy better than 0.5 m, and the convergence of the TWSTFT-based dynamic wide area differential correction model needs more than 300 min to obtain an accuracy better than 0.7 m.

The statistical biases achieved after a 24-hour static PPP are listed in Table 7.

It shows that centimeter-level positioning results can be achieved with IGS post-precise orbit and clock products, which also demonstrates that the PPP processing strategy is correct. After 24-hour static PPP, the positioning results can all reach the sub-meter level, with the dynamic wide area differential correction model being obviously better than the other two models. Because the dynamic wide area differential correction model uses phase observations directly, the kinematic wide area differential correction model only uses epoch differenced phase observations and still has residual tropospheric error. For the TWSTFT-based dynamic wide area differential correction model, there are systematic errors caused by the equipment time delay in satellite clock offset; as a result, the positioning result is worse than the dynamic wide area differential correction model.

6 CONCLUDING REMARKS

In this paper, we studied the orbit and clock differential correction methods for BDS SBAS, using kinematic, dynamic and TWSTFT-based dynamic models. The accuracies of UDRE, dual-frequency real-time positioning and PPP with the three differential correction models were compared. They show that dual-frequency real-time positioning accuracies with the three differential correction models are all below 2 meters, and are improved by 31%, 32% and 24% for the kinematic correction model,

Table 6 Summarizes the Strategy of PPP in the Paper

	Model	Strategy
Modeled observable	Measurements	Ionosphere-free combination: LC/PC
	Sampling interval	30 s
	Elevation cutoff	5°
	Weighting	LC: 0.01 m; PC: 1.00 m
	Adjustment	The Kalman filter
Error correction	Phase wind-up	Phase wind-up correction (Wu et al. 1992)
	Phase center offsets	Absolute IGS 08 correction mode
	Forces	Solid tide and Ocean tide correction
	Relativity	Applied
	Satellite orbit	Broadcast ephemeris with SBAS orbit corrections/IGS post-precise ephemeris fixed
	Satellite clock offset	Broadcast clock offsets with SBAS clock corrections/IGS post-precise clock products fixed
	Ionospheric delay	Corrected with dual frequency observation
Parameters	Station coordinates	Estimated
	Tropospheric delay	Estimated every three hours Mapping function: GMF (Böhm et al. 2006)
	Receiver clock offset	Estimated
	Ambiguity	Estimated

Table 7 A listing of 24-hour dual-frequency static PPP results with Open Service (OS), KIN, DYN, TSDYN, and IGS post precise satellite ephemeris and clock products (IGS).

Station	OS (m)	KIN (m)	DYN (m)	TSDYN (m)	IGS (m)
JFNG	1.22	0.45	0.15	0.54	0.02
SHA1	1.61	0.59	0.22	0.62	0.01
KUN1	1.18	0.46	0.17	0.55	0.01
GUA1	1.35	0.43	0.27	0.87	0.02
Chengdu	0.91	0.48	0.20	0.79	0.01
Harbin	1.54	0.34	0.34	0.63	0.01
Urumqi	1.77	0.67	0.27	0.74	0.01
Shantou	1.44	0.52	0.19	0.60	0.01
Average	1.38	0.49	0.23	0.67	0.01

dynamic correction model and TWSTFT-based dynamic correction model respectively, corresponding to open service. The dual-frequency real-time positioning accuracy of BDS SBAS is comparable with WAAS and EGNOS.

The PPP precision with the dynamic correction model is about 23 cm, and PPP precision with kinematic differential corrections and TWSTFT-based dynamic differential corrections may reach the sub-meter level. The reason for this may be due to the kinematic and TWSTFT-based dynamic correction models, but pseudorange data are still the main data resource when calculating the clock differential corrections. The results of the paper may be used as a reference for developing the new generation of BDS SBAS.

Acknowledgements The authors would like to thank the IGS for the provision of GPS observations, and precise GPS orbit and clock products used in this study. We also acknowledge the FAA Satellite Product Office for providing WAAS correction data and the ESA for the EGNOS correction data. This work is supported by the National Key Research Program of China as the "Collaborative Precision Positioning Project" (No. 2016YFB0501900), the National Natural Science Foundation of China (Grant Nos. 41674041, 41574029 and 11203059), the Youth Innovation Promotion Association CAS (Grant No. 2016242), Shanghai Science and Technology Committee Foundation (Grant No. 16511103003), and the Shanghai Key Laboratory

of Space Navigation and Position Techniques (Grant No. 12DZ2273300, ZZXT_201701).

References

BeiDou ICD. 2013, BeiDou Navigation Satellite System Signal in Space Interface Control Document Open Service Signal B1I (Version 1.0), China Satellite Navigation Office (CSNO)

Böhm, J., Niell, A., Tregoning, P., & Schuh, H. 2006, Geophysical Research Letters, 33

Cao, Y., Hu, X., Wu, B., et al. 2012, Science China Physics, Mechanics, and Astronomy, 55, 1307

Cao, Y., Hu, X., Zhou, J., et al. 2014, in China Satellite Navigation Conference (CSNC) 2014 Proceedings: Volume III, Springer, 277

Chao, Y. 1997, Real Time Implementation of the Wide Area Augmentation System for the Global Positioning System with an Emphasis on Ionospheric Modeling, PhD Thesis, Stanford University, California

Chen, J., Hu, Y., Zhang, Y. 2017, Tongji Daxue Xuebao/journal of Tongji University, 45, 1075

Heßelbarth, A., & Wanninger, L. 2013, GPS solutions, 17, 465

Labé, A. R., Lembachar, R., Authié, T., Trilles, S., & Mercier, F. 2016, in ION GNSS+ 2016, 1

Lawrence, D., Bunce, D., Mathur, N. G., & Sigler, C. E. 2007, in Proceedings of the 20th International Technical Meeting of the Satellite Division of The Institute of Navigation (ION GNSS 2007), Fort Worth, TX, 892

Liu, L., Zhu, L.-F., Han, C.-H., Liu, X.-P., & Li, C. 2009, Chinese Astronomy and Astrophysics, 33, 431

Manabe, H. 2008, in Proceedings of the 21st International Technical Meeting of the Satellite Division of the Institute of Navigation (ION GNSS 2008), Savannah, GA, 1032

Rho, H., & Langley, R. B. 2007, in Proceedings of the 20th International Technical Meeting of the Satellite Division of The Institute of Navigation (ION GNSS 2007), Fort Worth, TX, 939

Seynat, C., Flament, D., & Brocard, D. 2009, in Proceedings of the 22nd International Technical Meeting of The Satellite Division of the Institute of Navigation (ION GNSS 2009), Savannah, GA, 3457

Shi, C., Zheng, F., Lou, Y., et al. 2017, Remote Sensing, 9, 1

Tang, C., Hu, X., Zhou, S., et al. 2016, Advances in Space Research, 58, 1390

Tsai, Y. J. 1999, Wide Area Differential Operation of the Global Positioning System: Ephemeris and Clock Algorithms, PhD Thesis, Stanford University, California

Wu, J. T., Wu, S. C., Hajj, G. A., Bertiger, W. I., & Lichten, S. M. 1992, in Astrodynamics 1991; Proceedings of the AAS/AIAA Astrodynamics Conference, ed. P. A. Penzo & D. F. Bender, 1647

Zhou, S., Hu, X., Wu, B., et al. 2011, Science China Physics, Mechanics, and Astronomy, 54, 1089

Wu, X., Zhou, J., Wang, G., Hu, X., & Cao, Y. 2012, Science China Physics, Mechanics, and Astronomy, 55, 1297